Article

Heparin and methionine oxidation promote the formation of apolipoprotein A-I amyloid comprising #-helical and #-sheet structures.

David Townsend, Eleri Hughes, Rohanah Hussain, Giuliano Siligardi, Sara J. Baldock, Jillian Madine, and David A. Middleton

Biochemistry, **Just Accepted Manuscript** • DOI: 10.1021/acs.biochem.6b01120 • Publication Date (Web): 19 Dec 2016

Heparin and methionine oxidation promote the formation of apolipoprotein A-I amyloid comprising α-helical and β-sheet structures.

David Townsend[1], Eleri Hughes[1], Rohanah Hussain[2], Giuliano Siligardi[2], Sarah Baldock[1], Jillian Madine[3] and David A. Middleton[1*]

[1]Department of Chemistry, Lancaster University, Lancaster United Kingdom

[2]Diamond Light Source Ltd, Diamond House, Harwell Science & Innovation Campus, Didcot OX11 0DE, Oxon, England.

[3]Department of Biochemistry, Institute of Integrative Biology, University of Liverpool, United Kingdom

*Corresponding author:

David A. Middleton, Department of Chemistry, Lancaster University, Lancaster LA1 4YB, U.K.

E-mail: d.middleton@lancaster.ac.uk

Tel: +44 1524 594328

Keywords: ApoA-I, solid-state NMR, synchrotron radiation circular dichroism, atherosclerosis, amyloidosis, glycosaminoglycan, methionine oxidation.

Abbreviations: ApoA-I, ThT, HDL, TEM, AFM, CD, XRD, NMR, LDL, SRCD, SSNMR, LB, HIS, IPTG, EDTA

Structural analysis of apolipoprotein A-I aggregates

Abstract

Peptides derived from apolipoprotein A-I (apoA-I), the main component of high-density lipoprotein (HDL), constitute the main component of amyloid deposits that co-localise with atherosclerotic plaques. Here we investigate the molecular details of full-length, lipid-deprived apoA-I after assembly into insoluble aggregates under physiologically-relevant conditions known to induce aggregation *in vitro*. Unmodified apoA-I is shown to remain soluble at pH 7 for at least 3 days, retaining its native α-helical-rich structure. Upon acidification to pH 4, apoA-I rapidly assembles into insoluble non-fibrillar aggregates lacking the characteristic cross-beta features of amyloid. In the presence of heparin, the rate and thioflavin T responsiveness of the aggregates formed at pH 4 increase and short amyloid-like fibrils are observed, which give rise to amyloid-characteristic X-ray reflections at 4.7 and 10 Å. Solid-state NMR (SSNMR) and synchrotron radiation circular dichroism (SRCD) spectroscopy of fibrils formed in the presence of heparin retain some α-helical characteristics together with new β-sheet structures. Interestingly, SSNMR indicates a similar molecular structure of aggregates formed in the absence of heparin at pH 6 after oxidation of the three methionine residues, although their morphology is rather different from the heparin-derived fibrils. We propose a model for apoA-I aggregation in which perturbations of an 4-helix bundle-like structure, induced by interactions of heparin or methionine oxidation, cause the partially helical N-terminal residues to disengage from the remaining, intact helices, thereby allowing self-assembly via β-strand associations.

Structural analysis of apolipoprotein A-I aggregates

Atherosclerosis is a disease of the circulatory system initiated by the formation of plaques lining the arterial vessels composed of fibrous protein, cholesterol and extracellular matrix elements. Excess cholesterol, which can promote formation of these plaques, is removed from the circulatory system and transported to the liver for processing by the high-density lipoprotein (HDL) complex.[1, 2] The anti-atherogenic properties of HDL are attributed to their ability to stimulate cellular cholesterol efflux through the transport of cholesterol from the atherosclerotic lesions to the liver, as well as to inhibit low-density lipoprotein (LDL) oxidation and inflammatory events.[2] The main protein component of HDL is the 28-kDa, 243-residue apolipoprotein A-I (apoA-I), which accumulates cholesterol and phospholipids [3] and has high structural plasticity, adopting different conformational structures depending on whether it is lipid-deprived or associated with HDL particles. The lipid-deprived protein has a core 4-helix bundle-like structure and lipid-bound apoA-I forms a tetrameric twisted-ring of mostly of α-helices occasionally broken up by proline.[4-9] ApoA-I maintains the HDL structure and integrity by forming an anti-parallel helical double belt surrounding the lipids and cholesterol. About 95% of circulating plasma apoA-I exists as a stable α-helical conformation associated with HDL with the remainder in a labile lipid-deprived monomeric state.[10]

Lipid-deprived apoA-I variants can undergo an alternative folding pathway in which the protein self-assembles into β-sheet rich amyloid fibrils,[11, 12] resulting in loss of the HDL's atheroprotective mechanism, the accumulation of damaging plaques in vital organs and, potentially, excessive inflammation that has been shown to be induced by cytotoxic fibril intermediates.[13, 14] Hereditary forms of apoA-I amyloidosis are characterized pathologically by the deposition of 80-100 residue N-terminal peptide fragments derived from apoA-I mutants.[15-17] Several natural single point

mutations have been identified in the protein's N-terminal region and residues 170-178[14, 15, 18] and some, if not all, of these mutations destabilize the three-dimensional structure and ultimately expose regions to proteolytic cleavage.[19] Various N-terminal peptides have been shown to assemble into amyloid-like fibrils and bind the thioflavin T dye *in vitro* autonomously in the absence of the remaining apoA-I sequence.[20-22] A non-hereditary, acquired form of amyloidosis involving non-variant apoA-I has also been identified and is a common feature of lesions in atherosclerosis.[12, 23, 24] The atherosclerotic plaques incorporate full-length non-variant protein in addition to N-terminal peptide fragments.[12, 25, 26] A 100-fold increase in the amount of apoA-I in atherosclerotic arteries compared with normal arteries has been observed, and the protein deposits are fibrillar and cross-linked.[27, 28] The high incidence of fibrillar apoA-I associated with atherosclerotic lesions, along with their cytotoxicity and ability to activate arterial macrophages, suggest that amyloid deposition may decrease plaque stability and contribute to the progression of atherosclerosis.[14, 26, 29, 30]

The mechanism by which the native apoA-I assembles into the aggregates associated with atherosclerosis is not known, but studies of ApoA-I self-assembly *in vitro* suggest that the process is accelerated by three factors. Aggregation is more rapid under acidic conditions, which is consistent with the local decrease in extracellular pH under inflammation and in chronic hypoxic conditions.[30] The rate is also accelerated in the presence of heparin, a proxy for glycosaminoglycan (GAG) polysaccharides that are found associated with many different types of amyloid.[30] Interestingly, the GAG heparan sulfate prevented cytotoxic interactions of the G26R (Iowa) mutant with CHO cells.[31] Thirdly, oxidation of methionine residues has been shown to accelerate fibril deposition at normal physiological pH.[27, 28] Activated

macrophages in the atherosclerotic lesions secrete high levels of myeloperoxidase that oxidises apoA-I locally and reduces its anti-atherogenic function.[32]

Although there are several X-ray and solution structures published for non-aggregated apoA-I variants,[8, 33, 34] high-resolution structural details of apoA-I fibrils are currently lacking. It is not known whether the fibrils adopt a common structural architecture under the various conditions, or whether the structural plasticity of the protein results in diverse structural outcomes. In this work, we use high-resolution solid-state NMR and other methods to identify the structural features of aggregates formed by full-length, intact apoA-I and compare the structural composition of the aggregates formed at low pH, in the presence of heparin and after methionine oxidation.

Experimental Methods

ApoA-I expression

Expression of N-terminally His-tagged apoA-I was carried out by following previously published methods.[35, 36] A pNFXex expression vector coding for human apoA-I with an N-terminal His tag (kindly provided by Dr M. Oda, Oakland Research Institute, USA) was transformed into *E. coli* BL21 (DE3) cells (Agilent Technologies) and grown at 37°C in LB media containing 100 µg/ml ampicillin (Melford Laboratories). Once an OD_{600} of 0.6 was reached, protein expression was induced with 1 mM IPTG (Melford Laboratories) and incubated for 5 h. Transformed cells were also grown in minimal media incorporating ^{13}C glucose and ^{15}N ammonium chloride (99% purity, Cortecnet) as the sole carbon and nitrogen sources for analysis by solid-state NMR. Cells were harvested by centrifugation at 5,000 g for 20 minutes prior to re-suspension in cell lysis buffer (6 M GnHCl, 20 mM NaH_2PO_4, 0.5 M NaCl, pH 7.4)

and sonication at 20 microns in cycles of 25 %, to avoid overheating. Cell debris was removed through centrifugation at 43,000 g for 30 minutes before loading onto a 20 mL His Trap column (GE Healthcare) pre-equilibrated with lysis buffer. The column was washed with lysis buffer, binding buffer (20 mM NaH_2PO_4, 0.5 M NaCl pH 7.4) and binding buffer containing increasing concentrations of imidazole (25 mM and 50 mM). ApoA-I was eluted with 20 mM $NaPO_4$, 0.5 M NaCl, 500 mM imidazole and collected in 1 mL fractions. Fractions containing the highest protein content, measured by their absorbance at 260/280 nm, were pooled and dialysed against 4 L Tris buffer (20 mM Tris, 1 mM benzamidine, 1 mM EDTA pH 7) overnight. The protein was filtered using 0.2 μM filters (Corning) to remove any precipitate that formed during dialysis.

To facilitate removal of an N-terminal affinity tag used in protein isolation, the plasmid DNA contained a Glu2Asp mutation linker sequence NH_2-D^1DPPQS- with an acid-labile Asp2-Pro3 bond. The expressed protein was treated with 45 % formic acid at 55 °C for 5 hours to remove the His-tag by cleavage of the peptide bond between Asp-2 and Pro-3. Thus the protein lacks the native Glu-1 and Asp-2 residues. Two rounds of dialysis against Tris buffer were then carried out to remove the excess formic acid prior to dialysis against McIlvaine Buffer (165 mM Na_2HPO_4, 17.6 mM citrate, pH 7) and storage at -20 °C. The intact mass of apoA-I was confirmed by ESI mass spectrometry using a Waters Q-ToF micro system at a flow rate of 250 μL/hour via a syringe. The observed mass of 27,837 Da was in good agreement the expected mass of 27,834 Da.

Oxidation methods

ApoA-I was dialysed into 10 mM NaH_2PO_4 pH 7.5 overnight, prior to incubation with excess H_2O_2 (1000 fold molar excess) overnight at 37 °C. The

sample was then dialysed back into 10 mM NaH_2PO_4 pH 7.5 twice in order to remove any excess hydrogen peroxide.

Thioflavin T fluorescence and sedimentation measurements

Amyloid formation as measured by the enhancement of ThT (Sigma) fluorescence was carried out by a continuous read method, in which ThT was present during aggregation, and by a final read method in which ThT was added after a defined period. For continuous read, apoA-I (at 7 μM) was incubated in a 96-well clear-bottomed plate with agitation in McIlvaine buffer with 20 μM ThT in a total volume of 200 μL. Some solutions contained heparin (IdoA(2S)-GlcNS(6S) 14-15 kDa, >70 %, Iduron) at a twice the molar ratio to apoA-I. Fluorescence measurements were taken in triplicate using a Molecular Devices Flexstation 3 plate reader with excitation at 430 nm and emission at 480 nm every 30 seconds for 10 minutes, 2.5 μL of concentrated HCl was added to reduce the pH in wells that required a buffer of pH 4. Measurements were then taken every 30 seconds for 5 hours to monitor aggregation.

For the final read methods, apoA-I (36 μM) was incubated at pH 4 and pH 7 in the presence or absence of heparin. After 3 days' incubation, the sample was added to a 96-well plate along with 20 μM ThT and an end point fluorescence measurement taken with excitation at 430 nm and emission 480 nm. The samples were then removed from the plate and centrifuged at 13,400 rpm for 5 minutes in a bench-top centrifuge to pellet any aggregated material. The fluorescence of the supernatant was then measured. All measurements were performed in triplicate.

In experiments paralleling the final-read ThT measurements, apoA-I samples prepared under the same conditions but without ThT were centrifuged in a bench-top

centrifuge to sediment any aggregated material. The concentration of the protein remaining in the supernatant was measured using a Nanodrop 2000 (Thermo Scientific) and used to estimate the percentage of insoluble protein material.

Transmission Electron Microscopy

ApoA-I (36 μM) at pH 4, in the absence or presence of heparin (72 μM), was incubated at 37 °C for 3 days with agitation. Samples were pelleted and washed several times with distilled water to remove any buffer salts. Samples were diluted to 18 μM before 10 μL was loaded onto carbon coated copper grids and left for 2 minutes before excess sample was removed via blotting. The grid was then stained by inverting it onto a droplet of 0.2 % uranyl acetate. After 30 seconds of staining the grids were blotted and left to dry for 1 hour. The sample was then visualised on a Tecnai 10 electron microscope at 100 kV.

Atomic Force Microscopy

ApoA-I (36 μM) at pH 4, in the absence or presence of heparin at 72 μM, was incubated at 37 °C for 3 days with agitation. Samples were diluted to 18 μM and loaded onto freshly cleaved Mica surfaces and left to adhere to the membrane overnight. Samples were then washed with distilled water to remove any buffer salts. AFM was performed with a Keysight Technologies (Santa Rosa, Ca, USA) 5500 series instrument fitted with a 90x90 μm scanner. All images were acquired in acoustic alternating contact (AAC or “tapping”) mode using etched silicon probes (PPP-NCL, Keysight) with nominal fundamental resonance frequencies of 190 kHz. These 225 μm-long cantilevers have a nominal force constant (k) of 48 N/m and a top height of 10-15 nm and a tip radius of <10 nm. PicoView (V1.2, Keysight) was used to control the AFM and capture the images. Height (topographic), amplitude

and phase shift images were recorded simultaneously over an area of 0.5 x 0.5 μm at a frequency of 160 kHz,a scan rate of 0.5 lines/sec a setpoint (Asp) of 2.2 V. Analysis of images was performed using the Gwyddian V2.44 software.

Circular dichroism

ApoA-I (72 μM) at pH 7 and pH 4, in the absence and presence of heparin (144 μM), was incubated at 37 °C with agitation. It was necessary to use a higher concentration than in the analyses by other techniques to improve sensitivity, because a short path length (0.1 cm) cuvette was required to minimize interference from the buffer at wavelengths below 200 nm. Samples were taken at 0, 1 and 2 hour intervals and centrifuged at 13,400 rpm in a bench top centrifuge to pellet any insoluble material. The concentration of the supernatant was measured before loading into quartz cuvettes. SRCD experiments were performed between 185 and 260 nm, with a wavelength increment of 1 nm, using a nitrogen flushed Module X end-station spectrophotometer and the data analysed using CDApps [37] at B23 Synchrotron Radiation CD Beam line at the Diamond Light Source, Oxfordshire UK. Fitting was performed using the CONTINLL algorithm with dataset SMP 56 containing SP43 and 13 membrane proteins between the wavelengths of 190 and 250 nm. Samples of aggregated apoA-I formed at pH 4 in the absence and presence of heparin, from the solution circular dichroism experiments after 5 hours, were pelleted through centrifugation, deposited on Suprasil type quartz plates and dried under a stream of nitrogen at 23 °C to form a thin film. CD spectra were acquired between 180 and 260 nm using an integration time of 1 second and a bandwidth of 1.2 nm on a nitrogen flushed module B end-station spectrophotometer at B23 Synchrotron radiation CD beam line at Diamond Light Source, Oxfordshire UK. All

spectra presented are in the wavelength ranges that were unaffected by buffer interference and vary from sample to sample.

Thermal stability CD measurements were carried out using a ChiraScan Plus bench-top spectropolarimeter (Applied Photophysics) equipped with a quantium northwest temperature control. A temperature ramp from 20-90°C increasing at 1 degree per minute was applied and the temperature was held whilst the scan was taken from 180-260 nm. In all cases, background signals were removed from the spectra by subtraction of the appropriate spectrum of the buffer (+/- heparin) only.

X-ray diffraction

ApoA-I (36 μM) at pH 4, both in the absence and presence of heparin (72 μM), was incubated at 37 °C with agitation for 3 days. The fibrils were pelleted through centrifugation at 5,000 rpm into a glass capillary using a bench top centrifuge. The sample was irradiated using a Cu-Kα radiation (1.54 Å wavelength) and images were collected using a CCD detector (Atlas-S2).

Intrinsic fluorescence

ApoA-I at 18 μM at pH 4 and pH 7, in the absence and presence of heparin (36 μM), were incubated at 37 °C with agitation. Fluorescence spectra from 300 to 400 nm were collected on a Cary Eclipse spectrometer, with excitation at 279 nm and a band pass of 1 nm, immediately and 1 hour after preparation of the samples.

Sample preparation for solid-state NMR

Uniformly ^{13}C- and ^{15}N-labelled apoA-I (36 μM) was incubated for 3 days at pH 4 in the absence or presence of heparin (2:1 ratio of heparin to Apo AI). The fibrils were then pelleted by centrifugation at 13,400 rpm for 5 minutes and frozen using liquid nitrogen. The pellets were centrifuged into zirconium 3.2 mm NMR rotors fitted with Kel-F caps (Bruker, UK). In order to compare the spectra of insoluble fibrils with the

spectrum of native, soluble protein, uniformly labelled apoA-I was freshly prepared in pH 7 McIlvaine buffer and lyophilised before transferring into a 3.2 mm rotor.

Solid-state NMR methods

One dimensional proton-decoupled ^{15}N CP-MAS NMR experiments were performed at 25 °C using a Bruker Avance 400 MHz spectrometer (operating at a magnetic field of 9.3 T) equipped with a 3.2 mm HXY MAS probe. Hartmann-Hahn cross-polarization was achieved at a proton nutation frequency of 78 kHz with a contact times of 2 ms, 100 kHz proton decoupling with SPINAL-64[8] during signal acquisition and a recycle delay of 2 ms. Magic angle spinning was controlled at a frequency of 8 kHz +/- 1 Hz. Each spectrum was the result of accumulating 20,000-100,000 transients. Two dimensional ^{13}C-^{13}C spectra were recorded at 16.3 T with a 3.2 mm HXY probe operating in double-resonance mode and magic-angle spinning at 14 kHz. Samples were cooled to 4 °C. Hartmann-Hahn cross-polarization was achieved with a 2-ms contact time and 100-kHz proton decoupling with SPINAL-64 was applied during signal acquisition. For broadband dipolar recoupling, spectra were recorded with a 10-ms mixing time during which the proton nutation frequency was adjusted to the MAS frequency of 14 kHz to meet the dipolar-assisted rotational resonance (DARR) condition.[10] The time domain matrix was the result of 400 t_1 increments, each averaged over between 128 and 320 transients. Phase-sensitivity was achieved using the States-TPPI method. For selective dipolar recoupling, the proton nutation frequency was set to 100 kHz during a mixing time of 1-15 ms and the spinning frequency was adjusted to match the frequency difference of the nuclei to be recoupled.

Computational modelling

Homology modelling was carried out using Modeller version 9.13 and docking experiments were carried out using Molsoft ICM-Pro v 3.8-4a. Both methods used as the template the structural model of Δ(185-243)apoA-I. For docking analysis, a dp8 structural model of heparin previously reported [38] was used as the ligand. The initial docking region was defined by selection of the three histidine residues (H133, H153 and H160). Docking runs were performed with the histidine residues of MAβ40 in the default charge state (as generated by conversion of pdb files in ICM-Pro), and repeated with all histidines positively charged (HIP). Upon completion of docking hydrogen bonding interacions between ligand and receptor were observed.

Results

Heparin promotes the formation of amyloid-like apoA-I fibrils.

ApoA-I aggregation after incubation at 37°C with agitation for 3 days was monitored by end-point addition of the amyloid-diagnostic fluorescent dye thioflavin T (ThT) and also by quantifying the remaining protein following sedimentation and removal of insoluble material. ApoA-I aggregation is pH-dependent and both the yield of insoluble protein and ThT fluorescence increases with increasing acidity, with virtually no soluble protein remaining at pH 4 after 3 days (Figure S1A). However, transmission electron microscopy (TEM) reveals that the protein aggregates are non-fibrillar (Figure S1B). The ability of full-length de-lipidated apoA-I to form non-specific aggregates has long been known[39] and is probably a result of isoelectric precipitation around the native protein's pI of 5.17 (pI = 5.33 for the protein here, lacking the N-terminal Glu and Asp residues).

Structural analysis of apolipoprotein A-I aggregates

Glycosaminoglycan polysaccharides are believed to influence the accumulation and degradation of amyloid *in vivo.* These extracellular matrix components are well known to co-localize with amyloid, confer protease resistance on the amyloid deposits and enhance the rate of amyloid assembly.[40] The effect of GAGs on the rate of ApoA-I aggregation and on the aggregate morphology is here examined in the presence of 15 kDa heparin, a widely used proxy for cellular GAGs such as heparin sulfate.[41] A 2-fold molar excess of heparin has no additional effect on the amount of insoluble material produced after 3 days over a pH 4-8 range, compared to the protein alone (Figure 1A). By contrast, when apoA-I is incubated with heparin at pH 6 or lower, addition of ThT after 3 days results in a large additional enhancement of fluorescence, as compared to the protein in the absence of heparin (Figure 1B). The additional enhancement in the presence of heparin is not observed at pH 7 and pH 8, suggesting that heparin does not interact with the protein at neutral or mildly basic pH. It has been shown previously that heparin does not bind to apoA-I at neutral pH,[42] possibly because apoA-I lacks protonated histidine binding sites for the polyanion.

Continuous-read fluorescence measurements to monitor the time-course of aggregation in the presence of ThT confirms that apoA-I is stable at pH 7 with virtually no change in ThT fluorescence in the presence of heparin (data not presented). By contrast, addition of defined concentrations of heparin to the protein at pH 4 results in a rapid and immediate increase of ThT fluorescence in proportion to heparin concentration, followed by a slower exponential increase in fluorescence consistent with secondary nucleation catalysed by the surfaces of the rapidly-formed aggregates (Figure 1C).[43] The initial enhancement is reduced systematically with increasing salt concentration, indicative of an electrostatic interaction between

heparin and the protein (Figure S2). The rapid ThT increase is not consistent with stochastic nucleation of amyloid self-assembly, which is typically characterized by a lag-phase preceding rapid elongation, but implies that heparin promotes and directs the initial stages of protein self-assembly. The heparin concentration dependence of the initial fluorescence increase in Figure 1C could be fitted with a Hill equation giving an apparent dissociation constant (k_D) for heparin of 7.8 μM at pH 4. A similar effect of heparin is observed when stable solutions of protein and different concentrations of heparin at pH 7 are rapidly acidified by the addition of a calibrated volume of HCl (Figure S3), giving an apparent k_D of the same order of magnitude (2.6 μM).

TEM reveals the deposition of fine (<10 nm width) fibrillar structures at pH 4 in the presence of heparin, which are not observed in the absence of heparin (Figure 1D, left). Atomic force microscopy (AFM) also reveals networks of thin, amyloid-like fibrillar or protofibrillar species (Figure 1B, right). Taken together, these data suggest that heparin enhances the rate of formation and amyloid characteristics of apoA-I aggregates, but does not affect the final yield of insoluble material.

Different apoA-I aggregation pathways in the absence and presence of heparin.

The structural pathway of apoA-I aggregation was investigated by synchrotron radiation circular dichroism (SRCD).[44, 45] The SRCD spectrum of a fresh apoA-I solution at pH 7 is consistent with the high degree of α-helical structure (>50 %) of the native folded protein observed previously by far-UV CD [46] (Table 1), with characteristic minima at 208 nm and 222 nm. Subsequent spectra show that this structure remains stable for up to 5 h (Figure 2A). At pH 4, although a considerable amount of protein precipitation occurred, the remaining diluted solution of the protein

still retained significant amount of α-helical structure even after 2 h (insoluble material was removed by centrifugation before analysis) (Figure 2B). Fitting of the spectrum suggests a partial loss of helical content and gain in β-sheet and disordered elements (Table 1). In the presence of a 2-fold molar excess of heparin the intensity reduces considerably and it is no longer possible to discern the minima at 208 nm and 222 nm, although the signal-to-noise is now rather poor (Figure 2C). The solution spectra reflect only the structure of apoA-I remaining in the soluble form and do not report on the structure of the precipitated protein. We therefore isolated (by sedimentation and washing) the precipitated protein formed at pH 4 and obtained spectra of dried films of the precipitates only (Figure 3D). In the absence of heparin the spectrum is dominated by the typical α-helical features, but in the presence of heparin the minimum at ~222 nm is red-shifted to around 226 nm and the minimum at 208 nm reduces in intensity. Differential SRCD spectrum obtained by subtracting out the SRCD spectrum with heparin to that without heparin gave an indication of presence of >40% β-strand component using the CONTINLL algorithm (Figure 2D). [47] Further analysis using the BestSel algorithm [48] suggests the presence of β-strand of anti-parallel type. Virtually identical effects were observed for apoA-I aggregates formed after myeloperoxidase-catalysed oxidation of the methionine residues and these were attributed to increased β-sheet content.[27]

Intrinsic fluorescence of tryptophans 8, 50, 72 and 108 (Figure 3A) provided further details of the structural rearrangements accompanying apoA-I aggregation. At pH 7 in the presence or absence of heparin, the emission maximum occurs close to 337 nm in fresh solutions and after 2 h the maximum wavelength remains unchanged despite a loss of overall emission intensity, which may reflect some protein precipitation (Figure 3, B and C). Similar emission maxima are observed at

pH 4 in the absence of heparin, although the intensity reduction is considerably greater after 2 h, consistent with more rapid precipitation at the lower pH (Figure 3, D). In the presence of heparin the initial intensity is much lower than under the other conditions and suggests rapid protein precipitation followed by a slower rate over the subsequent 2 h (Figure 3E). A small blue shift to 335 nm occurs at pH 4 in the presence of heparin, which is not seen in the absence of heparin at pH 4 or when heparin is present at pH 7. The protein may undergo different structural rearrangements at pH 4 with heparin, which changes the environment(s) of one or more Trp residues. Typically, a blue shift indicates movement to a less polar environment and may also indicate movement of the fluorophore with respect to the positions of acidic and/or basic residues.[49] In the crystal structure of the C-terminally truncated variant Δ(185-243)apoA-I, tryptophans 6, 48 and 70 are close to arginine residues (59, 25 and 8, respectively) and a cation-π interaction between K23 and W50 is also observed. One or more of these interactions may be disrupted at pH 4 in the presence of heparin.

Heparin-catalysed ApoA-I fibrils comprise α-helical and β-sheet structural elements.

Cross-polarization magic-angle spinning (CP-MAS) solid-state NMR (SSNMR) is a powerful technique for resolving atomic details of amyloid fibrils [50], but so far it has not been applied to apoA-I fibrils. Here we used SSNMR to analyse in further detail the structure of the insoluble, uniformly ^{15}N- and ^{13}C-labelled apoA-I fibrils formed with heparin at pH 4. Spectra were obtained from hydrated insoluble fibrils after incubation for 3 days and compared with the SSNMR spectra of soluble protein at pH 7 after lyophilization. Chemical shifts for backbone ^{15}N and amide carbonyl (C'), Cα and Cβ positions are sensitive markers of local secondary structure. The backbone ^{15}N chemical shifts for the pH 7 sample are centred at ~119 ppm and

agrees with a simulated spectrum with chemical shifts predicted from the structure of Δ(185-243)apoA-I [8, 51] (Figure 4A, top). The spectrum is thus consistent with the 50-60 % α-helical content [46] of the natively-folded protein. The spectrum of fibrils formed at pH 4 in the presence of heparin is centred at ~121 ppm (Figure 4A, bottom), which indicates some structural perturbation from the α-helical-rich state. Amide ^{15}N chemical shifts for β-sheet and random coils are typically higher than the corresponding shifts for α-helical structures.[52]

Detailed structural differences between fibrillar and lyophilized protein are more evident when comparing two-dimensional ^{13}C-^{13}C SSNMR spectra of the two protein samples. Both spectra have rather broad lines (particularly for the lyophilized sample), consistent with a higher degree of heterogeneity than is seen in morphologically pure fibrils (e.g., Ref. [53]). This feature of the spectra, together with extensive peak overlap (a consequence of the size of the protein), prevented a full sequential assignment at this stage. The resolution was nevertheless sufficient to observe cross-peaks from several amino acid types (see below). The spectrum of the lyophilized protein again agrees well with a simulated spectrum based on predicted Cα, Cβ and backbone amide carbon (C') chemical shifts calculated from the crystal structure of Δ(185-243) apoA-I (Figure 4, B and C, left hand panels), and suggests that the protein retains predominantly its native helical structure after lyophilization. It should be recalled that here we are examining the full-length protein (except for residues 1-2) and so the spectrum also contains signal contributions from residues 185-243, which are absent from the crystal structure.[8] This region constitutes the lipid binding domain and is conformationally-variable, alternating between exposed disordered and more stable helical conformations depending on the association with lipids.[9] The readily-assigned Thr and Ser Cα-Cβ region of the

^{13}C-^{13}C spectrum may offer some insight into the structure of the C-terminal region. If the C-terminal region is unordered, well-resolved cross peaks for residues Thr-197, 200, 237 and 242 and residues Ser-201, 204, 224 and 228 would be expected around 61/71 ppm and 57/65 ppm respectively.[52] These are not evident in the spectrum. Cross-peaks for these residues in α-helical regions typically occur closer to the diagonal at 66/68 ppm and 61.63 ppm.[52] It is possible, therefore, that the C-terminal region adopts a partially α-helical conformation encompassing these residues, reflected in models presented elsewhere.[33]

The spectrum of the fibrillar protein at pH 4 (Figure 4, B and C, right hand panels) features several pronounced differences from that of the lyophilized protein, notably the appearance of several additional cross peaks for Ala, Val, Leu, Ser and Thr residues. One set of cross-peaks for these amino acids coincide with those for the lyophilized native protein, but the second set of cross-peaks occur at chemical shifts that are typical of local β-sheet conformations.[52] The Cα-Cβ cross-peaks occur at approximately 50.1-22.2 ppm for Ala (mean values of 50.9-21.7 ppm observed for β-sheet), 59.7-34.5 ppm for Val (60.7-33.8 ppm), 53.0-45.2 ppm for Leu (53.9-44.0 ppm), 55.7-65.2 ppm for Ser (57.1-65.4 ppm) and 60.3-70.1 ppm for Thr (61.1-70.8 ppm). Similar duplication of other cross-peaks may also occur, but could not be resolved. It appears that, unusually for amyloid-like fibrils, apoA-I comprises both secondary structural elements and the relative contour integrals suggest that at least 40 % of the above amino acids reside in β-sheet structures, although such quantitative analysis should be treated with caution. All five amino acids identified are distributed across the entire protein sequence, however, and so it is not possible to ascribe the β-sheet structures to a precise region of the protein.

Structural analysis of apolipoprotein A-I aggregates

ApoA-I residues 46-49 form β-sheet rich fibrils independently of heparin

Previous work identified a highly amyloidogenic N-terminal peptide fragment of apoA-I comprising residues L[49]LDNWDSVTSTFSK (ApoA-I(46-59)).[22] This sequence partially spans the unstructured region from Leu-40 to Thr-54 observed in the crystal structure of Δ(185-243)apoA-I.[8] We investigated whether heparin promotes self-assembly of this peptide, to establish whether the corresponding sequence in full-length apoA-I could form an interaction site for heparin. Coulomb repulsion between the two Asp residues of the peptide and the anionic sulfate and carboxylate groups of heparin may be negated by ionic interactions with the cationic C-terminal lysine and a possible array of hydrogen bonding interactions with polar residues along the peptide chain. The presence of hydrogen-bonding residues alongside lysine and arginine has been posited recently as being a characteristic feature of GAG binding sites in proteins.[54] Here, synthetic apoA-I(46-59) readily formed amyloid-like fibrils (~10 nm width) in the absence of heparin (Figure 5A) and SRCD revealed a concomitant structural rearrangement from mainly unordered to β-sheet after four hours incubation at 25 °C (Figure 5B). The minimum-to-maximum intensity transition around 194 nm after peptide aggregation is consistent with a conformational switch from an initial unfolded state to a predominantly β-sheet structure. A natural abundance ^{13}C SSNMR spectrum of unlabelled fibrils in the α-carbon region, which is sensitive to secondary structure, agrees well with a simulated spectrum for a peptide β-sheet and is inconsistent with other structures (Figure 5C and Figure S4). Peptide aggregation produces a rapid and large enhancement of ThT fluorescence, but, crucially, addition of a 2-fold excess of heparin does not have an appreciable effect on the rate of aggregation or on the apparent yield of fibrils as assessed by the end-point ThT fluorescence (Figure 5D).

These data indicate that although residues 46-59 are highly amyloidogenic and so may contribute to the self-assembly of apoA-I in the presence of heparin, they do not alone constitute a binding site for the GAG.

Methionine oxidized apoA-I fibrils are similar to heparin-induced fibrils.

Structural analysis of ApoA-I fibrils formed at low pH is relevant because apoA-I deposits accumulate under pro-inflammatory conditions that are associated with local acidification of the extracellular environment. The pH within plaques is heterogeneous and ranges from 7.5 to 5.5[55]. Nevertheless, the pathological pH is higher than the pH 4 conditions in which we observe apoA-I aggregation here. It has been shown that myeloperoxidase-catalysed oxidation by H_2O_2/Cl^- and enzyme-free chemical oxidation of apoA-I by H_2O_2 alone both modify methionine residues and accelerate the production of fibrillar amyloid within the atheromatous pH range.[27, 28] Activated macrophages in the atherosclerotic lesions secrete high levels of myeloperoxidase that oxidize apoA-I methionine residues and reduce anti-atherogenic function.[32] Here we incubated apoA-I in solution at pH 7 with a large molar excess (1000:1) of H_2O_2 to selectively oxidize methionine residues.[30] SDS-PAGE analysis confirmed that the protein remained intact after peroxide treatment (Figure 6A) and electrospray ionization (ESI) mass spectrometry indicated an increase in mass consistent with the oxidation of all three methionine residues (Met-86,112 and 148). CD measurements reveal differences in the thermal stability of unmodified and oxidized apoA-I (Figure S5). The unmodified protein undergoes a major structural change at around 56°C (Figure 6B), and qualitative analysis of the spectra suggest that partial unfolding of the predominantly α-helical structure occurs around this temperature, characterized by a shift in the CD minimum to 205 nm and loss of intensity around 222 nm (Figure 6C). The oxidized protein is much less stable

and undergoes major structural transitions at ~32°C and 70°C (Figure 6D). Qualitative analysis of the spectra indicates that below 32°C the protein retains its native, predominantly α-helical structure and between 32°C and 70°C the protein is in a partially unfolded state, (Figure 6E). Above 70°C the spectra are consistent with the protein regaining a partial helical structure. The secondary structural content could not be estimated reliably because it was not possible to determine the amount of protein precipitation during the thermal ramp.

The oxidized protein was incubated at pH 6 as described in previous work [27, 28] and readily and rapidly formed a visible white precipitate in the absence of heparin, whereas no such insoluble material was observed for non-oxidized protein under the same conditions. TEM revealed a mixture of long fibrillar structures (~10-20 nm width) and smaller spherical elements, possibly oligomers and/or protofibrils (Figure 7A). The ^{13}C-^{13}C spectrum of ^{13}C-labelled apoA-I aggregates produced under these oxidative conditions is highly similar to the spectrum of aggregates formed by unmodified protein in the presence of heparin (Figure 7B). Both spectra share the same characteristic cross-peaks for α-helical and β-sheet structures. It appears that apoA-I aggregation resulting from interactions with heparin at pH 4 or methionine oxidation at pH 6, involve the same core changes to the native protein structure.

Discussion

The current understanding of the aggregation of ApoA-I into amyloid *in vivo* is that the process results in the deposition of N-terminal fragments of apoA-I, 80-100 amino acids in length, and/or the full-length apoA-I. Familial apoA-I amyloidosis occurs when N-terminal fragments of mutant apoA-I species become deposited

within major organs,[14, 16, 18, 27, 56] whilst acquired amyloidosis is linked to the deposition of full-length amyloid within atherosclerotic plaques.[26, 30] The precise composition of the plaques and nature of the apoA-I species in atherosclerosis is only just coming to light.

Here we report the first detailed structural investigation of wild-type apoA-I aggregation under pro-inflammatory conditions. ApoA-I alone readily forms unordered aggregates in acidic medium, but in the presence of heparin at pH 4 the aggregation pathway is modified, resulting in short, ordered fibrillar structures giving the typical cross-beta diffraction spacings of amyloid. Surprisingly, the aggregates comprise both α-helical and β-sheet elements as revealed by solid-state NMR. Methionine oxidation results in longer ordered fibrils are formed alongside smaller spherical structures. Remarkably, despite the differences in the nanoscale morphologies of the heparin-promoted aggregates and the oxidized protein aggregates, their solid-state NMR spectra are virtually identical and consistent with the same structural features at the atomic level. What is not clear at this stage is whether the α- and β-structures represent entities that are structurally distinct (α-helical oligomers/protofibrils and β-sheet rich fibrils being one simplified example) or entities that are identical at the atomic level and comprising both structural elements within the single protein fold. We argue that the latter proposition is more likely: if structurally distinct aggregates were formed then one would expect their populations to vary under the different conditions of aggregation. The characteristic SSNMR peaks for the two secondary structures (which correspond approximately to their populations) are in the same proportions regardless of whether the aggregates are promoted at pH 4 by heparin at pH 4 or at pH 6 after protein oxidation. Similarly, their

proportions do not vary when heparin-induced aggregation is carried out at pH 5 or at a lower protein concentration of 18 μM (data not shown).

Louros and co-workers,[57] and Das and co-workers,[58] predicted three N-terminal amyloid-prone segments, residues 14-22, 53-58, 69-72, which in the native fold form an α-helical cluster, and the C-terminal residues 227-232. Structural perturbations in the amyloid-prone segments, induced by natural mutations associated with familial apoA-I amyloidosis, have been proposed to trigger a structural conversion in the N-terminal ~75 residues to form an intermolecular parallel β-sheet.[58] The positions of most naturally-occurring mutation sites, when mapped onto the crystal structure of the truncated protein Δ(185-243)apoA-I, support this model.[8, 19] Some mutations may initially cause only small perturbations in the native structure of the soluble protein, and it is subtle changes in attractive and repulsive side-chain interactions that appear to ultimately destabilize the protein, perhaps reducing the effect of residues protecting the major amyloid hot spot 14–22.[56, 58] It has been postulated that the sequence E^{76}KETEG act as a β-sheet breaker and, further, that protonation of the Glu residues under acidic pro-inflammatory conditions reduces this property and facilitates propagation of the β-sheet zipper from the N- to the C-terminus.[58] Although this process would reconcile all four amyloid hot spots in the full-length apoA-I, and expose the aggregates to protease cleavage, the SSNMR data clearly show that the fibrils retain an α-helical core and so do not support this hypothesis.

How do the diverse processes of methionine oxidation and heparin binding trigger the formation of ordered fibrils sharing a common structure? The mechanism of amyloid formation after methionine oxidation was discussed previously and the increased polarity of methionine sulfoxide probably disturbs the helix bundle packing and reduces structural stability in a similar way to non-polar to polar mutations L60R,

L64R and L178H.[58] Oxidation of Met-86 increased the amyloidogenic potential of the protein of destabilization[27] and this residue interacts with the predicted amyloid hotspot residues 14-22.[58] Oxidation could result in steric or electronic clashes with Tyr-16 promoting destabilization of the N-terminal helix. ApoA-I has a preponderance of basic residues free to participate in charge interactions with the polyanionic sulfate and carboxylate groups of heparin. The reduced effect of heparin around neutral pH suggests that protonated histidines may play a role in GAG binding. Three of the four histidines of apoA-I, His-135, 155 and 162, occur in the third extended helix, and we speculate that these residues, together with neighbouring Arg and Lys residues, promote heparin binding to the external surface presented by helices 2 and 3 (Figure S6).

In summary, apoA-I has a high propensity to aggregate at low pH, but interactions with GAGs of the extracellular matrix, or oxidation of methionine residues, are necessary to produce ordered fibrillar structures bearing the hallmarks of amyloid. SSNMR has revealed interesting and surprising new insights into the misfolding and amyloid formation of apoA-I, in particular that the amyloid species retain a high α-helical content. At present we can only apply these observations to apoA-I associated with acquired amyloidosis, but SSNMR may be used in future work to reveal similarities and/or differences in the aggregation pathways of the various apoA-I mutants associated with hereditary amyloidosis.

Acknowledgments

Dr Michael Oda (Children's Hospital, Oakland Research Institute) is kindly acknowledged for the donation of the pNFX expression vector. We thank Mr Mark Prescott (University of Liverpool) for assistance with mass spectroscopy.

Funding source material

This work was funded by the British Heart Foundation Project Grant FS/13/28/30208 (Studentship to DT).

Supporting Information

Supporting information available: further data on apoA-I aggregation, solid-state NMR data and molecular model diagrams.

References

[1] Annema, W., and von Eckardstein, A. (2013) High-Density Lipoproteins - Multifunctional but Vulnerable Protections from Atherosclerosis, *Circulation Journal 77*, 2432-2448.

[2] Fisher, E. A., Feig, J. E., Hewing, B., Hazen, S. L., and Smith, J. D. (2012) High-density lipoprotein function, dysfunction, and reverse cholesterol transport, *Arteriosclerosis, thrombosis, and vascular biology 32*, 2813-2820.

[3] Oram, J. F., and Vaughan, A. M. (2006) ATP-binding cassette cholesterol transporters and cardiovascular disease, *Circulation Research 99*, 1031-1043.

[4] Borhani, D. W., Rogers, D. P., Engler, J. A., and Brouillette, C. G. (1997) Crystal structure of truncated human apolipoprotein A-I suggests a lipid-bound conformation, *Proc. Natl. Acad. Sci. USA 94*, 12291-12296.

[5] Martin, D. D. O., Budamagunta, M. S., Ryan, R. O., Voss, J. C., and Oda, M. N. (2006) Apolipoprotein A-I assumes a "looped belt" conformation on reconstituted high density lipoprotein, *J. Biol. Chem. 281*, 20418-20426.

[6] Nath, A., Atkins, W. M., and Sligar, S. G. (2007) Applications of phospholipid bilayer nanodiscs in the study of membranes and membrane proteins, *Biochemistry 46*, 2059-2069.

[7] Segrest, J. P., Jones, M. K., Klon, A. E., Sheldahl, C. J., Hellinger, M., De Loof, H., and Harvey, S. C. (1999) A detailed molecular belt model for apolipoprotein A-I in discoidal high density lipoprotein, *J. Biol. Chem. 274*, 31755-31758.

[8] Mei, X. H., and Atkinson, D. (2011) Crystal Structure of C-terminal Truncated Apolipoprotein A-I Reveals the Assembly of High Density Lipoprotein (HDL) by Dimerization, *J. Biol. Chem. 286*, 38570-38582.

[9] Chetty, P. S., Mayne, L., Lund-Katz, S., Stranz, D., Englander, S. W., and Phillips, M. C. (2009) Helical structure and stability in human apolipoprotein A-I by hydrogen exchange and mass spectrometry, *Proc. Natl. Acad. Sci. USA 106*, 19005-19010.

[10] Rye, K. A., and Barter, P. J. (2004) Formation and metabolism of prebeta-migrating, lipid-poor apolipoprotein A-I, *Arteriosclerosis Thrombosis and Vascular Biology 24*, 421-428.

[11] Chiti, F., and Dobson, C. M. (2006) Protein misfolding, functional amyloid, and human disease, In *Annu. Rev. Biochem.*, pp 333-366.

[12] Mucchiano, G. I., Haggqvist, B., Sletten, K., and Westermark, P. (2001) Apolipoprotein A-I-derived amyloid in atherosclerotic plaques of the human aorta, *Journal of Pathology 193*, 270-275.

[13] Zhang, W., Wang, T. G., Pei, Z., Miller, D. S., Wu, X. F., Block, M. L., Wilson, B., Zhang, W. Q., Zhou, Y., Hong, J. S., and Zhang, J. (2005) Aggregated alpha-synuclein activates microglia: a process leading to disease progression in Parkinson's disease, *FASEB J. 19*, 533-542.

[14] Ramella, N. A., Schinella, G. R., Ferreira, S. T., Prieto, E. D., Vela, M. E., Luis Rios, J., Alejandra Tricerri, M., and Rimoldi, O. J. (2012) Human Apolipoprotein A-I Natural Variants: Molecular Mechanisms Underlying Amyloidogenic Propensity, *Plos One 7*.

[15] Obici, L., Franceschini, G., Calabresi, L., Giorgetti, S., Stoppini, M., Merlini, G., and Bellotti, V. (2006) Structure, function and amyloidogenic propensity of apolipoprotein A-1, *Amyloid-Journal of Protein Folding Disorders 13*, 191-205.

[16] Monti, D., Piccoli, R., and Arciello, A. (2011) *Apolipoprotein A-I Associated Amyloidoses: The Intriguing Case of a Natively Unfolded Protein Fragment, Amyloidosis - Mechanisms and Prospects for Therapy*.

[17] Rowczenio, D., Dogan, A., Theis, J. D., Vrana, J. A., Lachmann, H. J., Wechalekar, A. D., Gilbertson, J. A., Hunt, T., Gibbs, S. D. J., Sattianayagam, P. T., Pinney, J. H., Hawkins, P. N., and Gillmore, J. D. (2011) Amyloidogenicity and Clinical Phenotype Associated with Five Novel Mutations in Apolipoprotein A-I, *Am. J. Pathol. 179*, 1978-1987.

[18] Rosu, S. A., Rimoldi, O. J., Prieto, E. D., Curto, L. M., Delfino, J. M., Ramella, N. A., and Tricerri, M. A. (2015) Amyloidogenic Propensity of a Natural Variant of Human Apolipoprotein A-I: Stability and Interaction with Ligands, *Plos One 10*.

[19] Gursky, O., Mei, X., and Atkinson, D. (2012) The Crystal Structure of the C-Terminal Truncated Apolipoprotein A-I Sheds New Light on Amyloid Formation by the N-Terminal Fragment, *Biochemistry 51*, 10-18.

[20] Adachi, E., Kosaka, A., Tsuji, K., Mizuguchi, C., Kawashima, H., Shigenaga, A., Nagao, K., Akaji, K., Otaka, A., and Saito, H. (2014) The extreme N-terminal region of human apolipoprotein A-I has a strong propensity to form amyloid fibrils, *FEBS Lett. 588*, 389-394.

[21] Petrlova, J., Bhattacherjee, A., Boomsma, W., Wallin, S., Lagerstedt, J. O., and Irback, A. (2014) Conformational and aggregation properties of the 1-93 fragment of apolipoprotein A-I, *Protein Sci. 23*, 1559-1571.

[22] Wong, Y. Q., Binger, K. J., Howlett, G. J., and Griffin, M. D. W. (2012) Identification of an amyloid fibril forming peptide comprising residues 46-59 of apolipoprotein A-I, *FEBS Lett. 586*, 1754-1758.

[23] Westermark, P., Mucchiano, G., Marthin, T., Johnson, K. H., and Sletten, K. (1995) Apolipoprotein A1-Derived Amyloid in Human Aortic Atherosclerotic Plaques, *Am. J. Pathol. 147*, 1186-1192.

[24] Amarzguioui, M., Mucchiano, G., Haggqvist, B., Westermark, P., Kavlie, A., Sletten, K., and Prydz, H. (1998) Extensive intimal apolipoprotein A1-derived amyloid deposits in a patient with an apolipoprotein A1 mutation, *Biochem. Biophys. Res. Commun. 242*, 534-539.

[25] Loavenbruck, A. J., Chaudhry, V., Zeldenrust, S. R., Spinner, R. J., Theis, J. D., and Klein, C. J. (2012) Mass spectrometry analysis reveals non-mutated apolipoprotein a1 lumbosacral radiculoplexus amyloidoma, *Muscle & Nerve 46*, 817-822.

[26] Mucchiano, G. I., Jonasson, L., Haggqvist, B., Einarsson, E., and Westermark, P. (2001) Apolipoprotein A-I-derived amyloid in atherosclerosis - Its association with plasma levels of apolipoprotein A-I and cholesterol, *Am. J. Clin. Pathol. 115*, 298-303.

[27] Chan, G. K. L., Witkowski, A., Gantz, D. L., Zhang, T. O., Zanni, M. T., Jayaraman, S., and Cavigiolio, G. (2015) Myeloperoxidase-mediated Methionine Oxidation Promotes an Amyloidogenic Outcome for Apolipoprotein A-I, *J. Biol. Chem. 290*, 10958-10971.

[28] Wong, Y. Q., Binger, K. J., Howlett, G. J., and Griffin, M. D. W. (2010) Methionine oxidation induces amyloid fibril formation by full-length apolipoprotein A-I, *Proc. Natl. Acad. Sci. USA 107*, 1977-1982.

[29] Rocken, C., Tautenhahn, J. R., Buhling, F., Sachwitz, D., Vockler, S., Goette, A., and Burger, T. (2006) Prevalence and pathology of amyloid in atherosclerotic arteries, *Arteriosclerosis Thrombosis and Vascular Biology 26*, 676-677.

[30] Ramella, N. A., Rimoldi, O. J., Prieto, E. D., Schinella, G. R., Sanchez, S. A., Jaureguiberry, M. S., Vela, M. E., Ferreira, S. T., and Alejandra Tricerri, M.

(2011) Human Apolipoprotein A-I-Derived Amyloid: Its Association with Atherosclerosis, *Plos One 6*.

[31] Kuwabara, K., Nishitsuji, K., Uchimura, K., Hung, S. C., Mizuguchi, M., Nakajima, H., Mikawa, S., Kobayashi, N., Saito, H., and Sakashita, N. (2015) Cellular Interaction and Cytotoxicity of the Iowa Mutation of Apolipoprotein A-I (ApoA-I-Iowa) Amyloid Mediated by Sulfate Moieties of Heparan Sulfate, *J. Biol. Chem. 290*, 24210-24221.

[32] Nicholls, S. J., Zheng, L. M., and Hazen, S. L. (2005) Formation of dysfunctional high-density lipoprotein by myeloperoxidase, *Trends in Cardiovascular Medicine 15*, 212-219.

[33] Pollard, R. D., Fulp, B., Samuel, M. P., Sorci-Thomas, M. G., and Thomas, M. J. (2013) The Conformation of Lipid-Free Human Apolipoprotein A-I in Solution, *Biochemistry 52*, 9470-9481.

[34] Yang, Y. H., Hoyt, D., and Wang, J. J. (2007) A complete NMR spectral assignment of the lipid-free mouse apolipoprotein A-I (apoAI) C-terminal truncation mutant, apoAI(1-216), *Biomolecular Nmr Assignments 1*, 109-111.

[35] Ryan, R. O., Forte, T. M., and Oda, M. N. (2003) Optimized bacterial expression of human apolipoprotein A-I, *Protein Expression Purif. 27*, 98-103.

[36] Oda, M. N., Bielicki, J. K., Berger, T., and Forte, T. M. (2001) Cysteine substitutions in apolipoprotein A-I primary structure modulate paraoxonase activity, *Biochemistry 40*, 1710-1718.

[37] Hussain, R., Benning, K., Javorfi, T., Longo, E., Rudd, T. R., Pulford, B., and Siligardi, G. (2015) CDApps: integrated software for experimental planning and data processing at beamline B23, Diamond Light Source, *Journal of Synchrotron Radiation 22*, 465-468.

[38] Stewart, K. L., Hughes, E., Yates, E. A., Akien, G. R., Huang, T. Y., Lima, M. A., Rudd, T. R., Guerrini, M., Hung, S. C., Radford, S. E., and Middleton, D. A. (2016) Atomic Details of the Interactions of Glycosaminoglycans with Amyloid-beta Fibrils, *Journal of the American Chemical Society 138*, 8328-8331.

[39] Vitello, L. B., and Scanu, A. M. (1976) Studies on human-serum high-density lipoproteins - self association of apolipoprotein A-I in aqueous solutions *J. Biol. Chem. 251*, 1131-1136.

[40] Cohlberg, J. A., Li, J., Uversky, V. N., and Fink, A. L. (2002) Heparin and other glycosaminoglycans stimulate the formation of amyloid fibrils from alpha-synuclein in vitro, *Biochemistry 41*, 1502-1511.

[41] Duchesne, L., Tissot, B., Rudd, T. R., Dell, A., and Fernig, D. G. (2006) N-glycosylation of fibroblast growth factor receptor 1 regulates ligand and heparan sulfate co-receptor binding, *J. Biol. Chem. 281*, 27178-27189.

[42] Harel, A., Fainaru, M., Rubinstein, M., Tal, N., and Schwartz, M. (1990) Fist apolipoprotein A-I has heparin binding-activity - implication for nerve regeneration *Journal of Neurochemistry 55*, 1237-1243.

[43] Knowles, T. P. J., Vendruscolo, M., and Dobson, C. M. (2014) The amyloid state and its association with protein misfolding diseases, *Nature Reviews Molecular Cell Biology 15*, 384-396.

[44] Hussain, R., Javorfi, T. S., and Siligardi, G. (2012) Circular dichroism beamline B23 at the Diamond Light Source, *Journal of Synchrotron Radiation 19*, 132-135.

[45] Javorfi, T., Hussain, R., Myatt, D., and Siligardi, G. (2010) Measuring Circular Dichroism in a Capillary Cell Using the B23 Synchrotron Radiation CD Beamline at Diamond Light Source, *Chirality 22*, E149-E153.

[46] Saito, H., Dhanasekaran, P., Nguyen, D., Holvoet, P., Lund-Katz, S., and Phillips, M. C. (2003) Domain structure and lipid interaction in human apolipoproteins A-I and E, a general model, *J. Biol. Chem. 278*, 23227-23232.

[47] Provencher, S. W., and Glockner, J. (1981) Estimation of globular protein secondary structure from circular dichroism, *Biochemistry 20*, 33-37.

[48] Micsonai, A., Wien, F., Kernya, L., Lee, Y. H., Goto, Y., Refregiers, M., and Kardos, J. (2015) Accurate secondary structure prediction and fold recognition for circular dichroism spectroscopy, *Proc. Natl. Acad. Sci. USA 112*, E3095-E3103.

[49] Chen, Y., and Barkley, M. D. (1998) Toward understanding tryptophan fluorescence in proteins, *Biochemistry 37*, 9976-9982.

[50] Tycko, R. (2011) Solid-State NMR Studies of Amyloid Fibril Structure, In *Annual Review of Physical Chemistry, Vol 62* (Leone, S. R., Cremer, P. S., Groves, J. T., and Johnson, M. A., Eds.), pp 279-299.

[51] Han, B., Liu, Y. F., Ginzinger, S. W., and Wishart, D. S. (2011) SHIFTX2: significantly improved protein chemical shift prediction, *Journal of Biomolecular Nmr 50*, 43-57.

[52] Wang, Y. J., and Jardetzky, O. (2002) Probability-based protein secondary structure identification using combined NMR chemical-shift data, *Protein Sci. 11*, 852-861.

[53] Schutz, A. K., Vagt, T., Huber, M., Ovchinnikova, O. Y., Cadalbert, R., Wall, J., Guntert, P., Bockmann, A., Glockshuber, R., and Meier, B. H. (2015) Atomic-Resolution Three-Dimensional Structure of Amyloid beta Fibrils Bearing the Osaka Mutation, *Angewandte Chemie-International Edition 54*, 331-335.

[54] Sarkar, A., and Desai, U. R. (2015) A Simple Method for Discovering Druggable, Specific Glycosaminoglycan-Protein Systems. Elucidation of Key Principles from Heparin/Heparan Sulfate-Binding Proteins, *Plos One 10*.

[55] Naghavi, M., John, R., Naguib, S., Siadaty, M. S., Grasu, R., Kurian, K. C., van Winkle, W. B., Soller, B., Litovsky, S., Madjid, M., Willerson, J. T., and Casscells, W. (2002) pH heterogeneity of human and rabbit atherosclerotic plaques; a new insight into detection of vulnerable plaque, *Atherosclerosis 164*, 27-35.

[56] Das, M., Wilson, C. J., Mei, X. H., Wales, T. E., Engen, J. R., and Gursky, O. (2016) Structural Stability and Local Dynamics in Disease-Causing Mutants of Human Apolipoprotein A-I: What Makes the Protein Amyloidogenic?, *Journal of Molecular Biology 428*, 449-462.

[57] Louros, N. N., Tsiolaki, P. L., Griffin, M. D. W., Howlett, G. J., Hamodrakas, S. J., and Iconomidou, V. A. (2015) Chameleon 'aggregation-prone' segments of apoA-I: A model of amyloid fibrils formed in apoA-I amyloidosis, *Int. J. Biol. Macromol. 79*, 711-718.

[58] Das, M., Mei, X. H., Jayaraman, S., Atkinson, D., and Gursky, O. (2014) Amyloidogenic mutations in human apolipoprotein A-I are not necessarily destabilizing - a common mechanism of apolipoprotein A-I misfolding in familial amyloidosis and atherosclerosis, *FEBS J. 281*, 2525-2542.

Table 1. Summary of apoA-I secondary content calculated from SRCD spectra of protein solutions.

Conditions	Time (h)	Percentage secondary structure[a]			
		helix	β-sheet	turn	unordered
pH 7	0	65	8	13	14
	2	62	9	24	5
pH 7 + heparin	0	60	8	21	11
	2	65	9	14	12
pH 4	0	53	5	18	24
	2	61	16	21	2
pH 4 + heparin[b]	0	4	41	22	32
	2	19	8	16	57

[a] All normalised mean residual standard deviation (NMRSD) < 0.03 except where indicated. The estimation was carried out using CONTINLL [47] algorithm in the CDApps suite of programs [37].

[b] NMRSD = 0.6 for pH 4 + heparin.

Structural analysis of apolipoprotein A-I aggregates

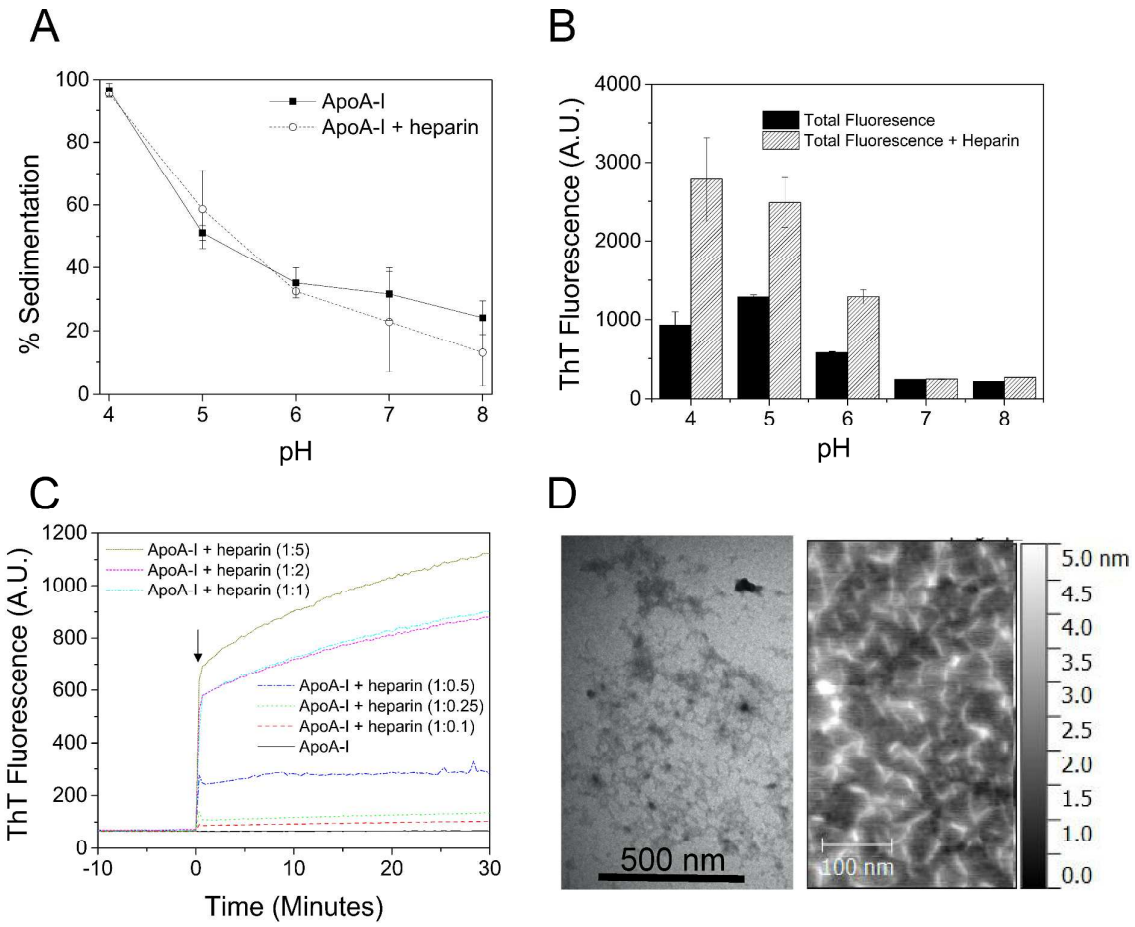

Figure 1. Enhancement of apoA-I aggregation by heparin. A: pH-dependence of insoluble protein formed after 3 days in the absence and presence of heparin (2-fold molar excess). B: pH-dependence of aggregation in the presence or absence of heparin measured by ThT fluorescence. C: Time-course of apoA-I aggregation at pH 4 (7 μM). All samples in figures A-C were for 10 minutes prior to addition of heparin (arrow). Mean and standard errors are shown in A, B and C for 3 samples per point. D: TEM (left) and AFM (right) characterization of apoA-I aggregates formed at pH 4 in the presence of heparin (2:1 molar ratio) after incubation for 3 days.

Structural analysis of apolipoprotein A-I aggregates

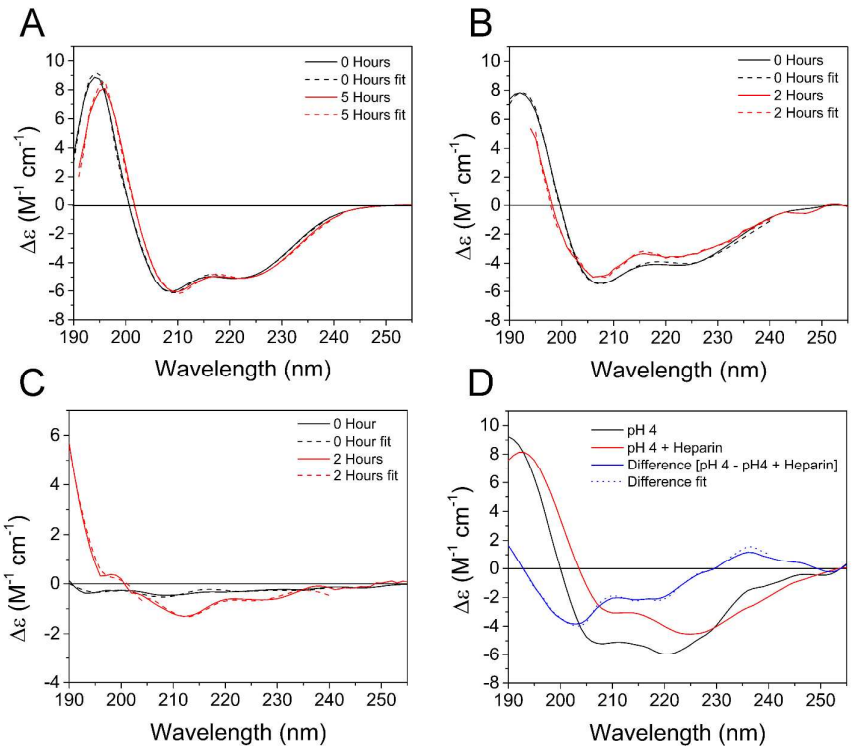

Figure 2. SRCD spectra of apoA-I (72 μM) in the absence or presence of heparin (2-fold molar excess). A: Spectra of apoA-I solutions at pH 7 in the absence of heparin, recorded after centrifugation to remove insoluble material. B: Spectra at pH 4 in the absence of heparin. C: Spectra at pH 4 in the presence of heparin. Dotted lines represent the best fits to the data using the CONTINLL algorithm. D: Spectra of dried films produced from apoA-I aggregates formed at pH 4 in the absence of heparin or with a 2-fold molar excess of heparin.

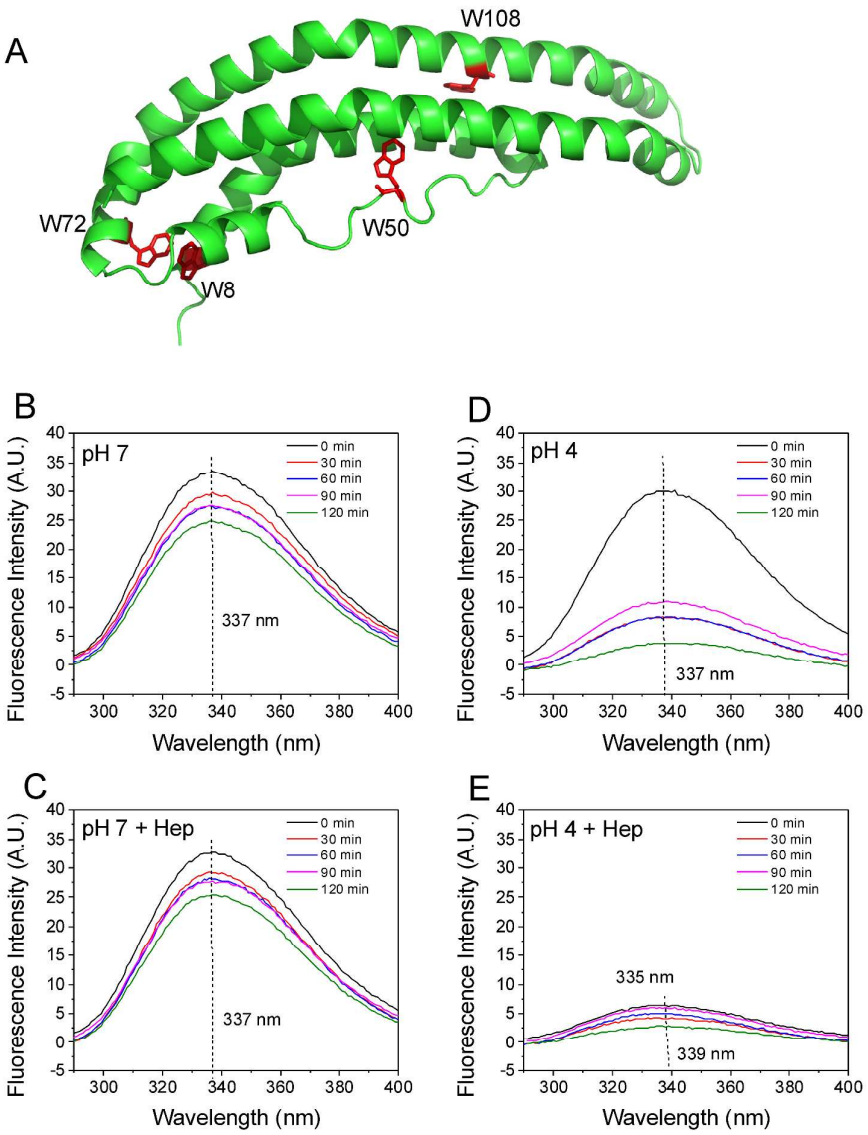

Figure 3. Time-dependence over 2 h of the intrinsic fluorescence emission of the four native apoA-I tryptophan residues. A: Structural model of residues 3-184 of natively folded monomeric apoA-I based on the crystal structure of the Δ(185-243)apoA-I domain-swapped dimer [8]. B: Spectrum at pH 7 alone. C: Spectrum at pH 7 with a 2-fold excess heparin. D: Spectrum at pH 4 alone. E: Spectrum at pH 4 with a 2-fold excess of heparin.

Structural analysis of apolipoprotein A-I aggregates

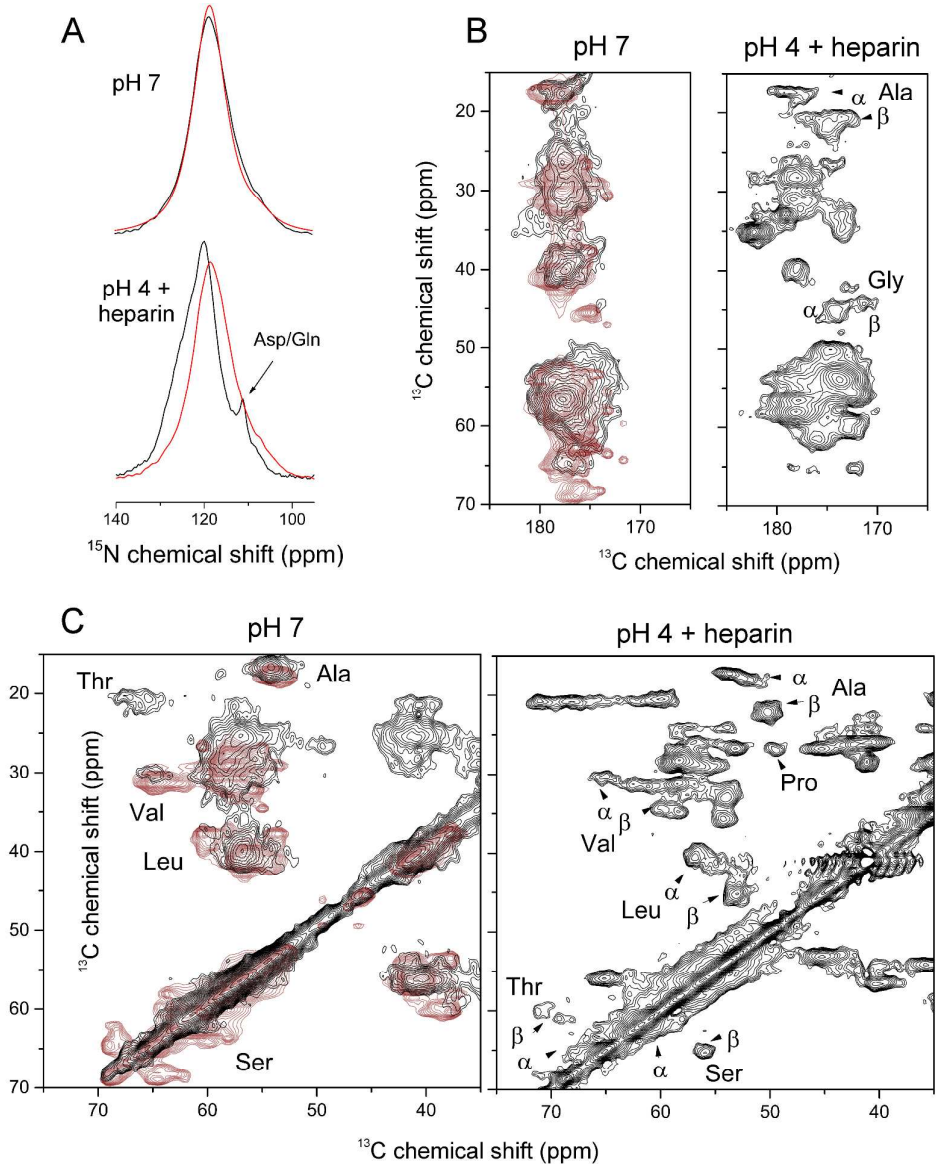

Figure 4. CP-MAS SSNMR spectra of apoA-I fibrils. Spectra were obtained for non-aggregated protein after lyophilization from a pH 7 solution and from a concentrated hydrated precipitate formed after 3 days of incubation at pH 4 in the presence of a 2-fold excess of heparin. The initial protein concentration was 36 μM in both cases. A: Backbone amide region of ^{15}N spectra. B: Amide region of 2D ^{13}C-^{13}C spectra. C: High-field region of the ^{13}C-^{13}C spectra. The annotation of some cross-peaks with α and β refer to assignments of the corresponding residues in α-helical and β-sheet conformations. Red lines and contours represent simulated spectra based on the model derived from the Δ(184-243)apoA-I structure [8] and were calculated from chemical shifts predicted by SHIFTX2 [51].

Structural analysis of apolipoprotein A-I aggregates

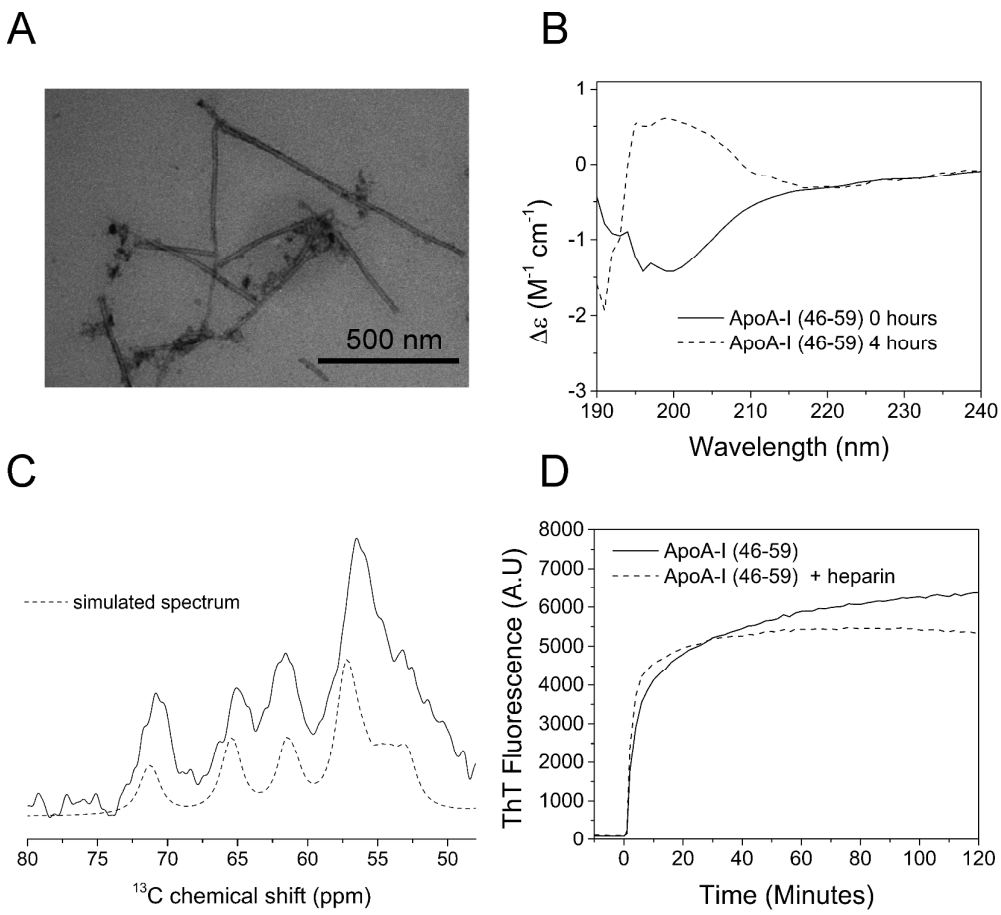

Figure 5. Aggregation of the apoA-I (46-59) peptide (1 mg/ml at pH 4). A: TEM image showing amyloid fibrils formed after 3 days. B: SRCD spectra of the peptide in solution initially (black) and after incubation at 25°C for 4 h with shaking (red). C: ^{13}C CP-MAS SSNMR spectrum of fibrils formed after 3 days. D: Thioflavin T fluorescence of the peptide alone and in the presence of a 2-fold excess of heparin.

Structural analysis of apolipoprotein A-I aggregates

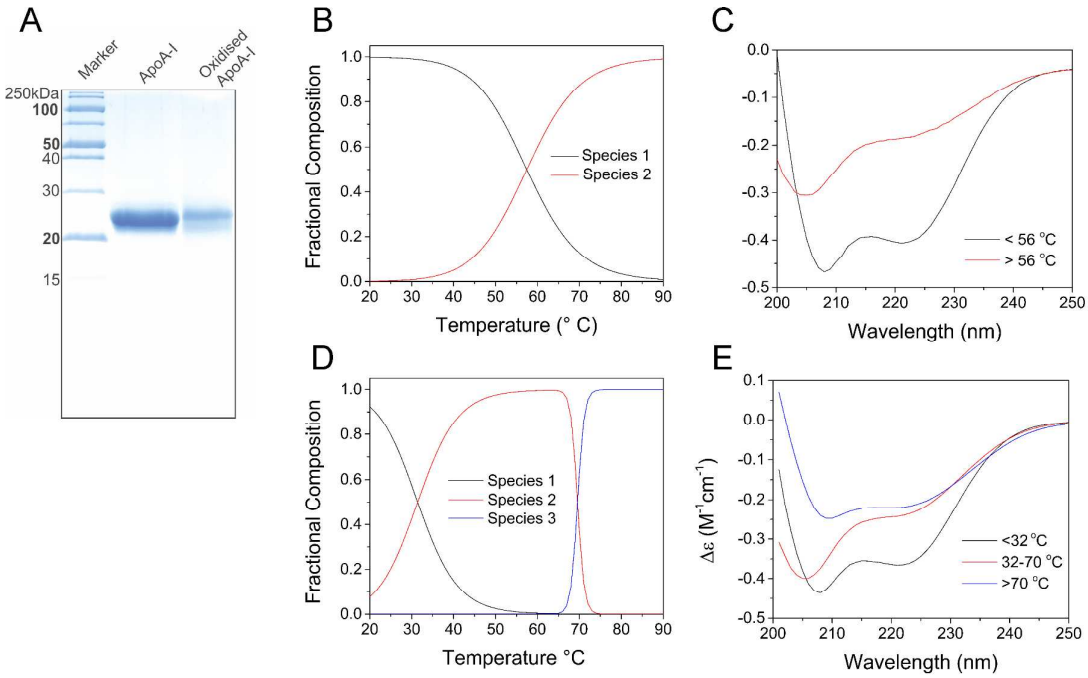

Figure 6. Characterization of soluble oxidized apoA-I. A: SDS-PAGE gel of apoA-I before and after oxidization by treatment with hydrogen peroxide. B: The thermal stability of unmodified apoA-I (72 μM) at pH 7 determined by CD. The fractional composition of two apoA-I species was determined by deconvolution of the CD spectra. C: CD spectra representing the principal components present below (black) and above (red) the transition temperature of 56°C. D: CD analysis of the thermal stability of oxidized apoA-I (72 μM) at pH 7 showing the fractional composition of three oxidized apoA-I species. E: CD spectra representing the principal components present below 32°C (black), between 32°C and 70°C (red) and above (blue) 70°C.

Structural analysis of apolipoprotein A-I aggregates

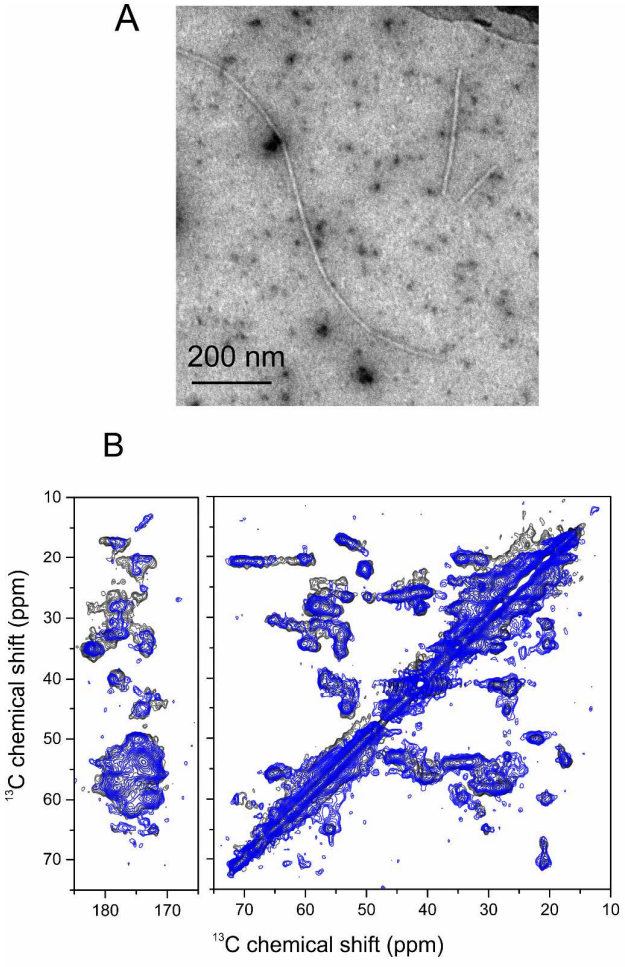

Figure 7. Characterization of insoluble oxidized apoA-I aggregates. A: TEM image of aggregates formed at pH 6 after apoA-I oxidation. B: Superimposed 2D ^{13}C-^{13}C SSNMR spectra of unmodified apoA-I aggregates formed at pH 4 in the presence of heparin (black) and oxidized apoA-I aggregates formed at pH 6 in the absence of heparin (blue).

For table of contents use only

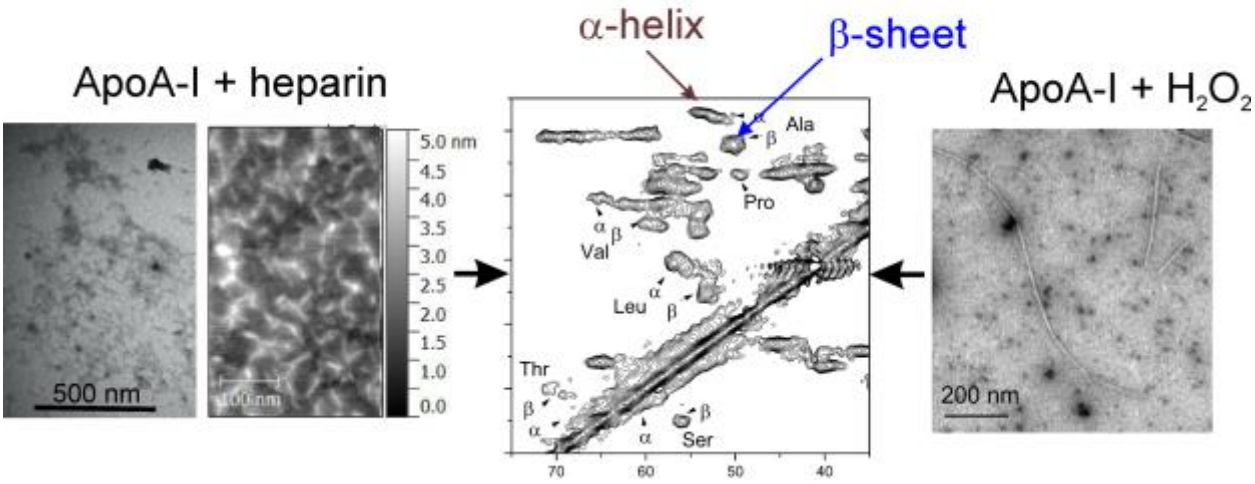

Heparin and methionine oxidation promote the formation of apolipoprotein A-I amyloid comprising α-helical and β-sheet structures.

David Townsend, Eleri Hughes, Rohanah Hussain, Giuliano Siligardi, Sarah Baldock, Jillian Madine and David A. Middleton*